Estuarine, Coastal and Shelf Science 241 (2020) 106813

Contents lists available at ScienceDirect

Estuarine, Coastal and Shelf Science

journal homepage: http://www.elsevier.com/locate/ecss

Examining the response of an eastern Australian mangrove forest to changes in hydro-period over the last century

Samuel K. Marx [a,*], Jon M. Knight [b], Patrick G. Dwyer [c], David P. Child [d], Michael A. C. Hotchkis [d], Atun Zawadzki [d]

[a] GeoQuEST Research Centre, School of Earth and Environmental Sciences, University of Wollongong, New South Wales, Australia
[b] Environmental Futures Research Institute, Griffith University, Nathan, Queensland, Australia
[c] Coastal Systems, DPI Fisheries, Wollongbar, New South Wales, Australia
[d] Institute for Environmental Research, Australian Nuclear Science and Technology Organisation, Sydney, New South Wales, Australia

ARTICLE INFO

Keywords:
Mangrove basin forest
Sea level rise
Substrate production
Fallout radionuclides
Anthropogenic change

ABSTRACT

This study examines mangrove substrate production within a mangrove basin forest in the Tweed Estuary, northern New South Wales, Australia. This is achieved using high resolution dating of $^{239+240}$Pu, ^{236}U and ^{210}Pb in mangrove sediments to examine both the modes and rates of mangrove substrate production. Results show a shift in the mode of substrate production occurred approximately 70 years ago in response to human modification of the Tweed Estuary (hydrologic changes). At that time, mangrove substrate production shifted from being dominated by sedimentation processes (fine silt accumulation) to being dominated by biological processes (mangrove root production). Since that time, mangrove peat has been accreting at the study site at the same rate as local sea level rise (SLR), implying current rates of peat substrate development are tuned to increasing sea level. A further implication of the shift to biological accretion at rates corresponding with SLR is that the studied mangrove basin is sequestering C at increasing rates due to subsurface root production.

1. Introduction

Mangrove forests occupy an area of coastline in excess of 137,000 km^2 globally, including 11,500 km^2 of the Australian coastline (approx. 18%) (Duke, 2006), where they provide a range of ecosystem services (Vo et al., 2012). These include providing habitat for both marine and terrestrial species, including humans (Vo et al., 2012), filtering deleterious terrestrial runoff (Wolanski, 2007), acting as a fish nursery (Faunce and Serafy, 2006) and protecting the coastline from wave erosion (Koch et al., 2009). In addition, mangroves are an important sink for atmospheric CO_2, sequestering amongst the highest proportions of C of any ecosystem (Alongi, 2014). Their habitat position, at the terrestrial-marine interface, is a highly dynamic geomorphic environment. Consequently, there is significant interest in understanding how mangroves respond to change (e.g., Laurance et al., 2011; Woodroffe, 2007), particularly sea level rise (SLR). Drowning or upslope migration were previously considered the most likely response of mangroves to SLR (Duke et al., 2007; Ellison, 1993; Ellison and Stoddart, 1991; Field, 1995; Woodroffe, 1990). Recent research indicates mangroves can be resilient to SLR (Lovelock et al., 2015; McKee et al., 2007), due to vertical accretion of mangrove substrate. This is due to either sedimentation (Lovelock et al., 2015) and/or subsurface biological production (Krauss et al., 2014; McKee et al., 2007). Therefore examining how mangrove substrate develops (Rogers et al., 2019) or collapses (Cahoon et al., 2003) in response to change is important for understanding mangrove resilience.

Mangrove basin forests are considered to be ecogeomorphic/biomorphodynamic systems (Murray et al., 2008; Twilley et al., 2019; Woodroffe et al., 2015). They comprise a characteristic geomorphic form consisting of a large central basin, in which mangrove forest grows, positioned landward of a coastal berm (levee) occupied by fringing mangroves (Knight et al., 2008; Lugo and Snedaker, 1974). Mangrove basin forests have been shown to occupy a specific hydro-dynamic position within the tidal prism as the berm precludes inundation by average high tides. In southern Queensland and northern New South Wales they are only flooded by high tides above the 80th, or 90th percentiles (Knight et al., 2008, 2009). The consistency of this hydro-dynamic position across different mangrove basin forests, implies

* Corresponding author.
E-mail address: smarx@uow.edu.au (S.K. Marx).

https://doi.org/10.1016/j.ecss.2020.106813
Received 29 August 2019; Received in revised form 13 March 2020; Accepted 29 April 2020
Available online 8 May 2020

that the berm, and associated basin, may be a biogeomorphic response to sea level (SL). That is, substrate growth occurs in response to sea level rise (SLR).

The relationship between mangroves and SL has resulted in mangroves being used as an indicator of SL change. Over millennial timescales (e.g., the Holocene), the age and position of mangrove roots and peat have been used to track the response of mangroves to SLR and to reconstruct SL histories (e.g. Beaman et al., 1994; Horton et al., 2005; Lewis et al., 2013; McKee et al., 2007; Scholl and Stuiver, 1967; Scholl et al., 1969; Sloss et al., 2007; Thom and Roy, 1985; Toscano and Macintyre, 2003; Woodroffe, 1981; Woodroffe et al., 1985). For example, fossil mangrove roots or substrate (mangrove peat) preserved above the intertidal has been used to infer past periods of higher sea level (most notably in the mid-Holocene) (Beaman et al., 1994; Horton et al., 2005; Scholl et al., 1969; Sloss et al., 2007; Thom and Roy, 1985; Woodroffe et al., 1985). Similarly, rates of mangrove substrate accumulation (McKee et al., 2007; Toscano and Macintyre, 2003; Woodroffe, 1981) and dating of submerged mangrove material have been used to infer SLR (e.g., Scholl and Stuiver, 1967; Scholl et al., 1969; Woodroffe et al., 1993). These studies demonstrate both the resilience of mangroves to SL change, for example, where mangrove peat indicates the continued presence of mangroves at sites experiencing SLR of up to 5.2 mm/yr during the Holocene (Toscano and Macintyre, 2003), and the potential for mangrove systems to collapse, e.g., where fossil mangrove material occurs below terrestrial sediments (see for example Lewis et al., 2013; Woodroffe et al., 2016).

Over shorter timescales (years to decades), a major investigative approach for assessing mangrove resilience to SLR has involved the use of surface elevation tables (SETs) (Boumans and Day, 1993; Cahoon et al., 2002; Lovelock et al., 2011, 2015; Rogers et al., 2006, 2014; Sasmito et al., 2016). These measure surface elevation change using a series of vertical pins attached, via a horizontal arm, to a central 'control' rod sunk deeply into the substrate (Cahoon et al., 2002). They are typically used alongside maker-bed horizons which measure accretion of sediment (Cahoon et al., 2002; Cahoon and Turner, 1989). SETs have yielded useful information on the response of mangrove substrate to SL change or other processes. These studies have shown surface elevation change in mangroves is a dynamic process that differs spatially and in time (McKee et al., 2007; Rogers et al., 2006). A limitation of SETs is that, to date, studies have been conducted over relatively short periods, typically less than ~20 years (Sasmito et al., 2016). At these time-scales, surface elevation can be influenced by transient conditions, e.g., changes in precipitation and/or variability in the water table (Rogers et al., 2014). In addition, while SETs measure the response of surface elevation they do not provide information on the actual subsurface processes operating. For example, sedimentation versus subsurface biological production, or compaction due to oxidation versus dewatering. Despite their usefulness, the limitations of SETs demonstrate there remains a need to examine the response of mangrove substrate to change directly, that is, within the substrate profile and over longer time-scales (Breithaupt et al., 2018).

The application of high resolution geochronology to date sediment cores extracted from mangrove substrate is another approach for examining mangrove responses to changing conditions. It can produce longer records (multi-decadal to centennial timescales) than are currently available from SET studies. Studies of mangrove substrate also have the advantage of providing information on specific processes, such as peat growth versus mineral sedimentation. A number of studies have employed the use of short-lived radionuclides, (^{210}Pb, often in combination with fallout radionuclides ^{137}Cs and more recently $^{239+240}$Pu) to examine rates of change in mangrove substrate (Lynch et al., 1989; Pérez et al., 2017; Sanders et al., 2010; Smoak et al., 2013). Such studies have been undertaken in a range of locations, including in the Gulf of Mexico/Florida (Hancock et al., 2011; Lynch et al., 1989; Smoak et al., 2013), New Zealand (Lynch et al., 1989; Pérez et al., 2017), Australia (Rogers et al., 2019) and Brazil (Lynch et al., 1989; Pérez et al., 2017; Sanders et al., 2010; Smoak et al., 2013). Despite this, there remains a paucity of data from many locations, including from Australia, where there are few studies of mangrove sedimentation over timescales greater than a few decades. Consequently, there is a critical lack of data on the response of Australian mangroves to SRL over the last century (Breithaupt et al., 2018; Church and White, 2011).

In this study the modes and rates of substrate production in a mangrove basin forest, in northern New South Wales, Australia, are examined. This is achieved by collecting and analysing sediment cores which are dated at high resolution using ^{210}Pb and fallout radionuclides ($^{239+240}$Pu and ^{236}U) allowing substrate accretion modes and rates to be determined. Results are then compared to rates of SLR over the past century in order to investigate how the mangrove basin forest is responding to SLR. Lastly, the implications of substrate accretion for C storage are investigated.

2. Methods

2.1. Study setting

Mangrove substrate growth rates were examined within a 25 ha subtropical mangrove forest located in Terranora Broadwater (28.229°S, 153.504°E), northern New South Wales, Australia (Fig. 1). The studied mangrove basin forest is tidally connected to a shallow estuarine lagoon (the Terranora Broadwater). The site is part of the Tweed River estuary, a 22 km^2 wave dominated barrier estuary with a trained (open) entrance and a catchment of 1054 km^2. The study site

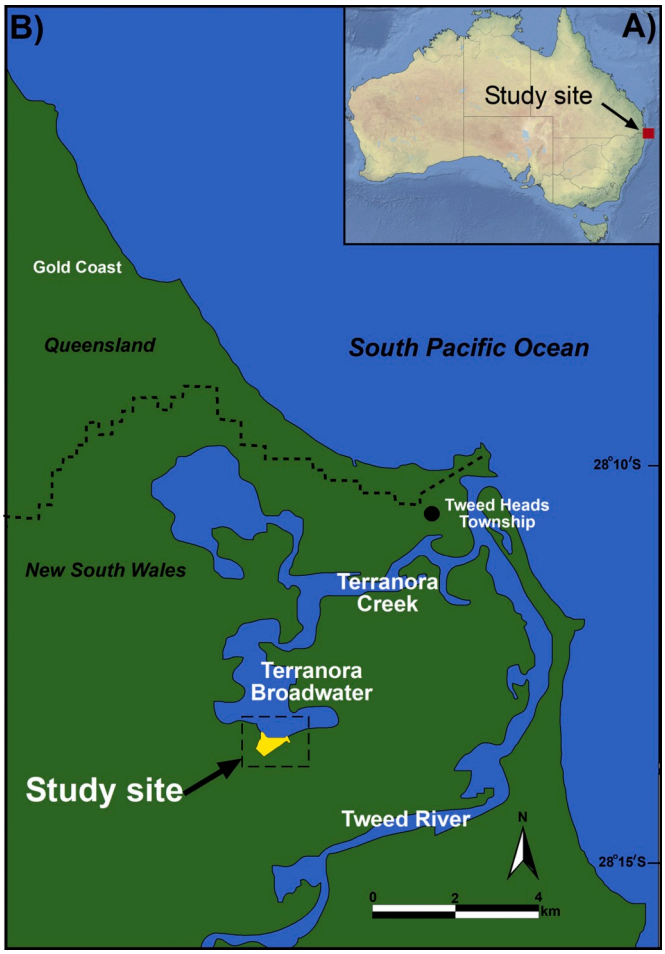

Fig. 1. A) The position of the study site in northern New South Wales, B) Location map showing the studied mangrove basin in Terranora Broadwater in the lower Tweed River estuary.

represents a mangrove basin forest (sensu Lugo and Snedaker, 1974), also referred to as interior mangroves (Krauss et al., 2014), consisting almost exclusively of the Grey Mangrove (*Avicennia marina var. australasica* (Walp.)). Grey mangroves have a dense root structure, consisting of cable roots growing radially from the trunk at shallow depths in the substrate (5–10 cm) and extending laterally up to >25 m (Knight et al., 2008). Pneumatophores grow vertically from cable roots and extend above the ground surface, reaching densities >1360/m^2 (Knight et al., 2008). Below the surface, pneumatophores grow fibrous lateral roots (feeding roots). These commonly interweave to form a continuous rootmat contributing to substrate mass (Baylis, 1950; Purnobasuki, 2013). As the root system is adventitious (meaning roots may grow from non-root material) the Grey Mangrove can rapidly produce root mass, with root production linked to tidal inundation of any part of the plant (Baylis, 1950; Parkinson et al., 1994). As is typical of mangrove basin forests, the studied basin contains sub-environments (micro--geomorphic/topographic features), which influence tidal inundation and ecological processes, e.g. mosquito production (Knight et al., 2012; Knight, 2011). These include hummocked areas of dense pneumatophores and open pools (with mud substrate). A prominent ridge runs through the centre of the basin (likely a palaeo fluvial levee), perpendicular to Terranora Broadwater (Fig. 2A and B).

2.2. Core collection and processing

Four cores were extracted from within the mangrove basin using a 1.8 m length 63 mm internal width gauge auger. Cores were collected to a depth where a sand sheet, underlying the upper mangrove silt/peat, was encountered. The cores were collected from differing sub-environments in the basin to capture potential heterogeneity in substrate accretion. This included from mangrove substrate (mud/pneumatophores) (TBC6), within pools (TBC1 and TBC5) and from topographic highs (the central basin ridge) (TBC7) (Fig. 2B). Core TBC6 was an 884 mm deep core that was extracted from mangrove substrate toward the terrestrial edge of the basin forest (Fig. 2A and B). It is representative of the majority of substrate and the main geomorphic structure of the basin and is therefore considered the master-core. It underwent more extensive dating and sediment analysis compared to the other cores and is predominately discussed. TBC1 (600 mm deep) was extracted from a pool at the back of the study site, while TBC5 (1670 mm deep) was collected from a large pool directly behind the berm. Core TBC7 (900 depth) was collected from pneumatophore dominated mangrove substrate from the ridge in the centre of the basin (Fig. 2).

Collected cores were placed in PVC core cradles and wrapped in plastic for transport and storage in a cool store at 5 °C. In the laboratory, cores were described and sectioned at 5 mm resolution using a stainless steel scalpel to slice the core into successive segments. Each segment was stored in vials in the cool store prior to additional analysis. The organic matter content of subsamples through the core was determined using loss on ignition at 450 °C. Dry bulk density was determined by volume displacement in water using plastic wrapped samples. Organic content was converted to C content using a 50% conversion factor (Pribyl, 2010). Grain size of selected samples through the cores was determined by laser diffraction using a Malvern Mastersizer 2000. These data were used to characterise the substrate type and were used for ^{210}Pb concentration corrections.

2.3. Core chronology

Geochronology of all four collected cores was determined by ^{210}Pb dating. Additional age control of the master-core, TBC6, was provided by measuring the fallout radionuclides $^{240+239}$Pu and ^{236}U. Fourteen samples were selected within the top 500 mm of TBC6 for ^{210}Pb dating. Similarly, eight samples were dated from TBC1 and TBC7, while 12 were dated from TBC5.

Lead-210 was determined by measuring ^{210}Po activity, with which ^{210}Pb is assumed to be in secular equilibrium. Unsupported ^{210}Pb was

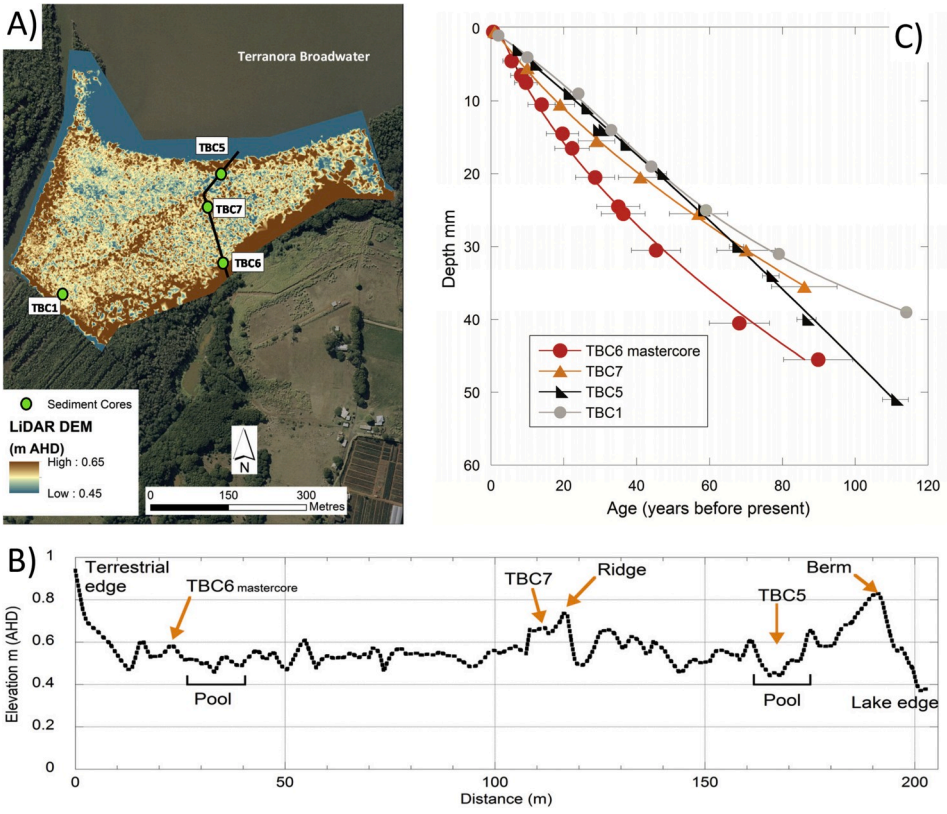

Fig. 2. Geomorphic structure of study site. A) Satellite image of the study site overlain by a LiDAR derived digital elevation model. The locations from where cores were collected is indicated by the green dots. The black line represents the position of a topographic transect across the study site plotted in B). The position of pools and the locations of cores is also indicated in panel B). C) Age depth profiles for the cores extracted from the study site. Plotted ages were derived using the CRC ^{210}Pb age model in each case. The fitted curves are 2nd order polynomial functions for TBC1, TBC5 and TBC7 and a 3rd order polynomial function for TBC6. (For interpretation of the references to colour in this figure legend, the reader is referred to the Web version of this article.)

calculated as the difference between total ^{210}Pb activity and that of ^{226}Ra, which was also measured in each sample. Prior to analysis samples were spiked with ^{133}Ba and ^{209}Po before being digested in HNO_3, H_2O_2 and HCl to extract ^{226}Ra and ^{210}Po from the sample matrix. Polonium-209 + 210 were auto-deposited onto silver disks and counted by high resolution Alpha Spectrometry. Radium-226 and ^{133}Ba were co-precipitated with barium sulfate ($BaSO_4$) and collected on membrane filters. Barium-133 was counted on a High Purity Germanium (HPGe) Gamma Detector, while ^{226}Ra activity was determined by high resolution Alpha Spectrometry. Sediment ages were determined from unsupported ^{210}Pb activity using both the Constant Initial Concentration (CIC) (Robbins and Edgington, 1975) and the Constant Rate of Supply (CRS) (Appleby and Oldfield, 1978) models. Sample ages were corrected for moisture content and dry bulk density.

Fallout plutonium and uranium isotopes were analysed in 12 samples through the top 500 mm of TBC6. Isotopes were leached from the samples using sub-boiling aqua regia. Plutonium-242 (NIST SRM-4334H) and ^{233}U (NBL CRM 111-A) were added as isotope dilution tracers. Purification of plutonium and uranium from the bulk matrix was then achieved by ion exchange chromatography using stacked Eichrom® TEVA and UTEVA cartridges (50–100 μm) (Child et al., 2008). Plutonium and U fractions were co-precipitated separately with iron hydroxide (2.5 mg Fe), dried, calcined at 600 °C and loaded into AMS targets for analysis. AMS analysis was performed on ANSTO's VEGA accelerator, with both Pu and U analysed at 1 MV in the 3+ charge state. Further details of the method have been previously published (Wilcken et al., 2015).

Vertical substrate growth rates for TBC6 were calculated by fitting a 3rd order polynomial function to the ^{210}Pb age/depth data, creating an age model for the core. Core growth rate uncertainty was calculated from the difference between the ^{210}Pb ages and fallout radionuclides ages.

2.4. Sea level data and hydro-period analysis

Sea level records to compare with substrate accretion rates in the studied mangrove basin are available from regional and local tide gauges. Regional SL records include from Fort Denison, Sydney Harbour (Bureau of Meteorology), Australia's longest SL record (reliable data available from 1914), >600 km south of the study site and from the Australian Baseline Sea Level Monitoring Project (ABSLMP) sites at Rosslyn Bay and Port Kembla (National Tide Centre, 2012). These are the closest ABSLMP sites to the study site at 625 and 735 km distant, respectively. ABSLMP data commenced in the late 1990s and are the most accurate SL records from Australia as they are corrected for gauge subsidence and climate variability. Locally relevant SL data are available from the Gold Coast Sea Way (28 km distant) and the Brisbane Bar (~100 km distant) (www.bom.gov.au).

Tidal flooding frequency statistics for the study site were calculated for the Terranora Broadwater using data from the Tweed River Terranora tide gauge station (AWRC No. 201447). This consisted of 18,968 high-tide observations for the period 12/1987 to 6/2016 (data provided by Manly Hydraulics Laboratory; NSW Office of Environment of Environment & Heritage). Site tidal-flooding patterns were related to the adjacent Terranora station using pressure loggers (Rugged Troll 100 data loggers, Insitu, Colorado, USA). These were deployed for various periods between 2010 and 2015. Logger data were corrected for atmospheric variability and calibrated for water depth during deployment. Site flooding patterns were compared with a site digital terrain model derived from high-resolution LiDAR data (provided by Tweed Shire Council) and processed as outlined in Knight et al. (2009). This allowed the elevation of the berm to be determined and subsequently allowed calculation of the tidal exceedance level for the study site.

3. Results

3.1. Sedimentary characteristics of the mangrove basin

Three main sedimentary units were identified in the master-core (TBC6) (Fig. 3B). A medium grey sand occurred from the base of the core (884 mm depth) until 830 mm. This was overlain by grey silt (830-400 mm). Above the silt was a transition zone (400-300 mm) that graded into brown fibrous peat, characterised by a high concentration of small roots, but also including a palaeo-pneumatophore (Fig. 3A and B). The top 10–15 mm of the core consisted of highly reduced black peat, typically described as monosulfidic black ooze (MBO). Overall, the core was characterised by decreasing bulk density and increasing organic content toward the surface (Fig. 3C). Organic content of the silt layer was <30% content by weight, while bulk density was 0.7 g/m^3. In the transition zone, above the silt, organic matter increased to ~30% and bulk density was 0.2 g/m^3, reflecting increased root matter content in the core (Fig. 3C). In the peat unit, organic matter reached 50–70% of sample mass and bulk density was 0.1–0.14 g/m^3.

The stratigraphy of TBC7, from the ridge in the centre of the basin (Fig. 2A and B), broadly matched the master-core. This 900 mm core consisted of 500 mm of organic silt, overlain by a 100 mm transition unit. Above the transition unit the core contained silty peat between 400 and 190 mm depth. This was overlain by an increasingly organic peat (above 190 mm depth), with an approximately 5 mm MBO unit at the top of the core. TBC5, collected from the seaward-most pool at the lowest point in the mangrove basin, was 1670 mm deep (Fig. 2B). It consisted of a basal unit of coarse grey sand (1670–780 mm depth) containing shell fragments. Between 780 and 300 mm the sediment was more fine textured (slit), more organic (10–20% by weight) and darker in colour. From 300 mm the core organic content increased to >25%, increasing again to >37% in the top 200 mm of the core. At 200 mm, the sediment became browner with roots and occasional partly decayed pneumatophores present. Above 150 mm the core comprised an organic rich, black MBO, overlain by a 2 mm deep orange surface oxidised unit. Core TBC1, from a pool at the back of the study site (Fig. 2A and B), was 600 mm deep and contained a similar, although condensed (due to its higher elevation) sedimentary structure to TBC5. It comprised of a grey sand layer (organic content <10%) (600-510 mm depth), overlain by an increasingly silt rich unit (510-380 mm). Between 380 and 170 mm the core became increasingly brown in colour and more organic (average 17%). Above 170 mm, the organic content increased above 30% with the sediment browner in colour and more fibrous (due to the presence of roots). The top of the core above 85 mm consists of MBO with a 2 mm oxidised surface layer.

3.2. Dating

Unsupported ^{210}Pb activity in 14 independent samples from core TBC6 consistently declined with depth (Fig. 3D). Minor deviation in the age/activity profile at 100 and 170 mm depth was attributed to input of sediment with a different initial ^{210}Pb activity, or minor translocation of ^{210}Pb within the core. Despite these slight deviations, the unsupported ^{210}Pb structure indicates the core was highly amenable to ^{210}Pb dating. Lead-210 ages were modelled using both standard age models, the Constant Initial Concentration (CIC) and Constant Rate of Supply (CRS) models. Results from both models were near identical (Fig. 3E), implying the sedimentation rate and the ^{210}Pb flux to the basin have been broadly constant.

Unsupported ^{210}Pb activity in the three other cores collected from the studied mangrove basin (TBC1, 5 and 7) also showed a consistent decline with depth, albeit with two perturbations in the profile of TBC5 (Table 1). This indicated these three cores were also suitable for ^{210}Pb dating. Similar to the master-core, the CRC and CIC age models yielded identical results for TBC7 (from the central ridge). For the two pool cores, TBC1 and TBC5, the CIC model resulted in younger ages in the

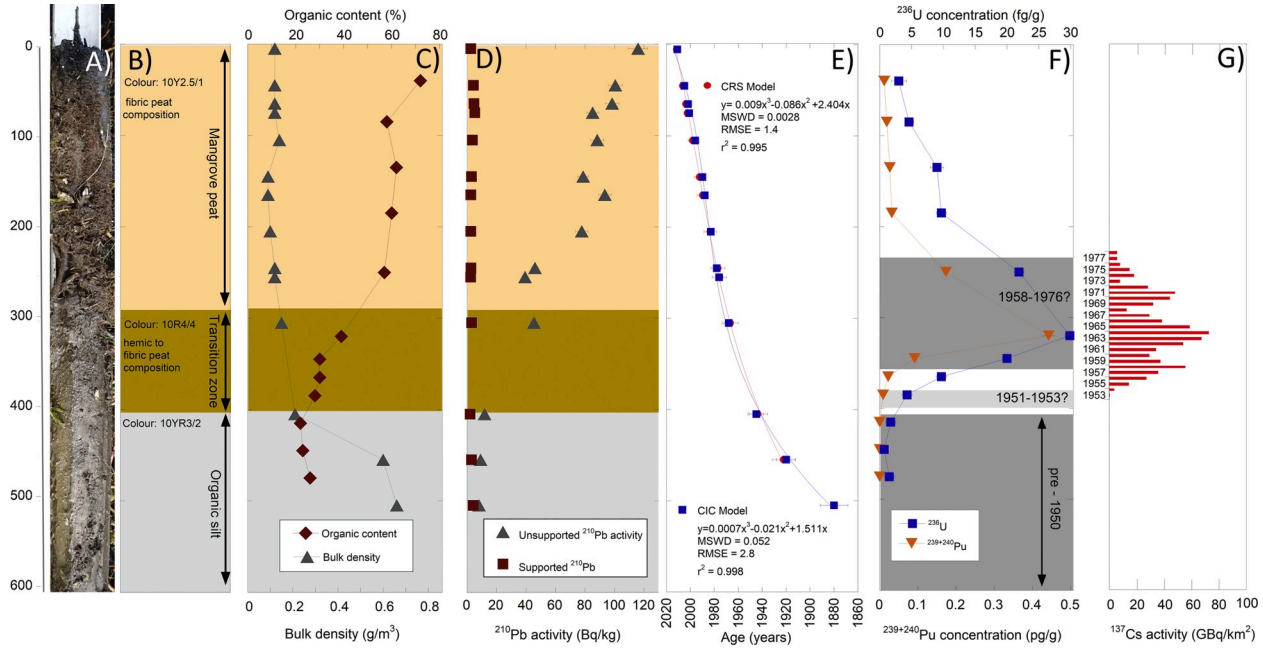

Fig. 3. Sedimentology and geochronology of the master-core, TBC6. A) Photograph of the core. B) The main stratigraphic units. C) Organic content and bulk density. D) Supported and unsupported ^{210}Pb profiles. E) The ^{210}Pb age-depth relationship derived from the CIC and the CRS age models. Fitted cures represent 3rd order polynomials. Curve equations, Root Mean Squared Error (RMSE), Mean Squares Weighted Deviation (MSWD) and r^2 values are indicated on the panel. F) Concentrations of fallout radionuclides $^{239+240}$Pb and ^{236}U through the sediment profile. G) Atmospheric ^{137}Cs fallout activity in Brisbane, 100 km from the study site (Longmore et al., 1983).

deepest samples relative to the CRC age model. These were close to error for TBC1 (40 mm depth CRS = 114 ± 1 years, CIC = 98 ± 11 years), but more significant in TBC5 (52 mm depth CRS = 93 ± 3 years, CIC = 135 ± 11 years). Greater complexity in ages in the pool cores reflects their more complex depositional environment. They receive both primary sediment input and secondary sediment input from the mangrove substrate adjacent to them.

The age structure of TBC6 (the master core) was further investigated using $^{240+239}$Pu and ^{236}U fallout radionuclides (Fig. 3F). Concentrations of both $^{240+239}$Pu and ^{236}U exhibit the same topology through the core, although the environmental concentration of ^{236}U is much lower than that of $^{240+239}$Pu. Samples below 400 mm depth contain negligible $^{240+239}$Pu and ^{236}U concentrations. Concentrations increased above 380 mm depth (more obviously for Pu initially), increasing more rapidly after 336 mm, and reaching a pronounced peak at 320 mm. Above this, concentrations decrease until 185 mm, from where they decease more significantly toward the top of the core.

The pattern of $^{240+239}$Pu and ^{236}U concentrations in TBC6 generally match the temporal pattern of atmospheric ^{137}Cs fallout measured in Brisbane (~100 km north) (Longmore et al., 1983) (Fig. 3G). However, $^{240+239}$Pu and ^{236}U concentrations in the core display less variability than recorded in atmospheric ^{137}Cs activity. This is likely due to the resolution at which the core was sampled, although it may also reflect minor mobility (smoothing) of $^{240+239}$Pu and ^{236}U concentrations within the core. Despite this, the broad agreement between atmospheric ^{137}Cs and $^{240+239}$Pu and ^{236}U in the core indicates fallout radionuclides are useful chronostratigraphic markers in this context.

3.3. Calculation of substrate accretion rates

The polynomial functions applied to the ^{210}Pb CRS and CIC age/depth data in TBC6 precisely fit the data, returning r^2 values of 0.99 and RMSE values of 1.4 and 2.8 (Fig. 3E). This indicates core accretion rates can be accurately calculated. The accuracy and precision of the ^{210}Pb age model can be further examined using fallout radionuclides. These provide independent chronology for the core. Plutonium isotopes ($^{239+240}$Pu) are becoming increasingly established as chronostratigraphic markers (Zheng et al., 2008) due to their greater prevalence and ease of detection compared to ^{137}Cs (Hancock et al., 2011). Similarly, ^{236}U has a common source from bomb fallout and therefore potentially a shared distribution, albeit at lower concentrations. Studies have begun to investigate ^{236}U as a chronostratigraphic maker (Ketterer et al., 2013; Srncik et al., 2014; Wendel et al., 2013).

Fallout $^{240+239}$Pu and ^{236}U provide two chronostratigraphic tie points in sediment cores; i) initial onset of fallout accumulation (1951–1953) and ii) peak fallout (1963). This allows identification of four zones in TBC6. These are; i) the pre-fallout period (pre-1950), ii) fallout onset (1951–1953), iii) peak fallout (1963) and, iv) declining fallout (post-1980). The age/depth structure of these zones in TBC6 conform to the ^{210}Pb dates (Fig. 3). The onset of increasing $^{240+239}$Pu and ^{236}U concentrations occurs at 365–390 mm depth, equating to 1952 CE (Longmore et al., 1983; UNSCEAR, 2000). The ^{210}Pb age models predict this depth range equates to the years 1947–1956 CE or 1945–1952 CE for the CIC and CRS models (Fig. 3). Peak bomb fallout $^{240+239}$Pu and ^{236}U concentrations at 310–330 mm depth representing the year ~1963 (Longmore et al., 1983; UNSCEAR, 2000). The equivalent date in ^{210}Pb space is 1965–1970 and 1960–1966 for the CIC and CRS models. Therefore, the two dating systems are in agreement indicating core accretion rates can be reliably calculated. Minor differences between the two systems likely represent the sampling resolution, or minor mobility in ^{210}Pb and Pu, which is possible in some cases (Field et al., 2018; Kaplan et al., 2006; Urban et al., 1990).

Using the polynomial function, fitted to the ^{210}Pb age/depth data from TBC6, substrate accretion rates were calculated, while the difference between ^{210}Pb ages and fallout chronostratigraphic ages were used to calculate uncertainty. Resulting average substrate accretion rates are 4.1 ± 0.3 and 4.5 ± 0.005 mm/yr for the CIC and CRC age models over the past ~120 years. Growth rates are increased toward the present reaching 7.8 ± 1.2 and 7.2 ± 0.007 mm/yr after 1990 CE. The other cores show similar growth rates, but with some variability. TBC7 displays growth rates of 3.7 mm/yr over the last 120, years increasing to 5.0 mm/yr since 1990 (Fig. 2C). Growth rates in the two pool cores

Table 1
^{210}Pb activity, ages and mass accumulation rates in collected sediment cores.

Core	Average depth (mm)	Total ^{210}PFb (mm)	Supported ^{210}Pb (Bq/kg)	Unsupported ^{210}Pb (Bq/kg)	Age CIC (Years)	Age CRS (Years)	CRS MAR (g/m^2/yr)
TBC6	5	123.3 ± 6.8	2.5 ± 0.3	121.0 ± 6.9	0.8 ± 0.4	0.6 ± 0.8	0.10 ± 0.01
	45	108.6 ± 5.0	4.4 ± 0.6	105.0 ± 5.0	6.8 ± 0.4	5.7 ± 2.4	0.09 ± 0.01
	65	105.3 ± 4.7	4.7 ± 0.4	102.7 ± 4.8	9.8 ± 0.5	8.3 ± 2.9	0.09 ± 0.01
	75	93.6 ± 4.2	5.3 ± 0.6	89.0 ± 4.2	11.3 ± 0.5	9.6 ± 3.1	0.10 ± 0.01
	105	95.6 ± 4.6	3.6 ± 0.4	92.1 ± 4.6	16.2 ± 0.7	13.9 ± 3.7	0.08 ± 0.01
	145	83.5 ± 3.8	3.0 ± 0.3	82.2 ± 3.9	21.9 ± 0.9	19.7 ± 4.4	0.08 ± 0.01
	165	98.0 ± 4.4	2.6 ± 0.3	97.5 ± 4.5	24.2 ± 1.1	22.3 ± 4.7	0.06 ± 0.01
	205	83.6 ± 4.4	2.6 ± 0.3	81.2 ± 4.4	29.0 ± 1.3	28.6 ± 5.3	0.06 ± 0.01
	245	49.7 ± 2.5	2.7 ± 0.3	48.1 ± 2.5	34.5 ± 1.6	35.0 ± 5.9	0.08 ± 0.01
	255	43.2 ± 2.1	2.5 ± 0.3	41.0 ± 2.1	36.0 ± 1.7	36.3 ± 6.0	0.09 ± 0.01
	305	50.1 ± 2.3	3.1 ± 0.3	47.4 ± 2.4	44.4 ± 2.5	45.3 ± 6.7	0.06 ± 0.01
	405	14.5 ± 0.6	2.1 ± 0.3	12.4 ± 0.7	67.0 ± 4.8	68.2 ± 8.3	0.11 ± 0.02
	455	12.3 ± 0.5	2.9 ± 0.3	9.6 ± 0.6	92.4 ± 6.2	89.8 ± 9.5	0.07 ± 0.02
	505	12.4 ± 0.6	4.1 ± 0.4	8.5 ± 0.7	131.9 ± 7.9		
TBC7	5	98.6 ± 5.2	3.1 ± 0.3	95.8 ± 5.3	1.0 ± 1.0	0.8 ± 0.9	0.19 ± 0.01
	55	95.2 ± 4.5	3.9 ± 0.4	91.4 ± 4.5	11.1 ± 1.2	9.6 ± 3.1	0.15 ± 0.01
	105	69.5 ± 2.9	4.7 ± 0.7	65.0 ± 3.0	21.2 ± 1.5	19.2 ± 4.4	0.16 ± 0.01
	155	48.0 ± 1.8	0.9 ± 0.2	47.5 ± 1.9	31.3 ± 2.0	28.5 ± 5.3	0.16 ± 0.01
	205	42.9 ± 1.9	3.9 ± 0.4	39.1 ± 2.0	43.9 ± 2.6	41.2 ± 6.4	0.13 ± 0.01
	255	22.7 ± 0.9	3.1 ± 0.3	19.8 ± 0.9	59.1 ± 3.4	56.6 ± 7.5	0.16 ± 0.02
	305	16.3 ± 0.7	3.8 ± 0.4	12.6 ± 0.8	74.2 ± 4.2	70.2 ± 8.4	0.17 ± 0.02
	355	14.2 ± 0.6	3.2 ± 0.3	11.0 ± 0.7	89.4 ± 5.0	86.2 ± 9.3	0.12 ± 0.02
TBC5	30	157.7 ± 3.3	3.8 ± 0.5	156.0 ± 3.4	6.3 ± 2.2	6.4 ± 0.18	0.22 ± 0.01
	50	105.8 ± 4.0	3.2 ± 0.3	103.0 ± 4.0	10.5 ± 2.3	10.4 ± 0.39	0.30 ± 0.01
	90	90.6 ± 3.2	2.8 ± 0.2	88.1 ± 3.3	19.8 ± 2.7	18.1 ± 0.66	0.27 ± 0.01
	110	80.6 ± 2.1	3.0 ± 0.5	78.6 ± 2.2	24.9 ± 3.0	22.5 ± 0.80	0.27 ± 0.01
	135	48.4 ± 1.5	4.1 ± 0.5	44.9 ± 1.6	31.2 ± 4.2	27.4 ± 0.94	0.40 ± 0.02
	135	42.4 ± 2.0	3.1 ± 0.4	39.3 ± 2.0	31.2 ± 2.7	27.4 ± 0.94	0.46 ± 0.03
	162.5	74.6 ± 3.0	3.5 ± 0.3	71.4 ± 3.1	38.2 ± 4.2	32.7 ± 1.10	0.21 ± 0.01
	195	54.6 ± 2.7	5.9 ± 0.6	48.8 ± 2.7	46.4 ± 3.8	41.4 ± 1.37	0.24 ± 0.02
	247.5	20.2 ± 0.7	4.3 ± 0.4	16.0 ± 0.8	59.7 ± 5.0	50.6 ± 1.67	0.55 ± 0.04
	247.5	23.6 ± 0.8	6.6 ± 0.6	17.2 ± 1.0	59.7 ± 5.0	50.6 ± 1.67	0.51 ± 0.04
	295	28.5 ± 1.3	6.0 ± 0.6	22.4 ± 1.4	72.7 ± 5.8	58.5 ± 1.95	0.30 ± 0.03
	340	15.8 ± 0.7	5.7 ± 0.4	10.2 ± 0.9	85.9 ± 7.2	66.6 ± 2.27	0.52 ± 0.05
	400	14.3 ± 0.6	6.5 ± 0.5	7.9 ± 0.8	103.7 ± 8.5	74.7 ± 2.63	0.52 ± 0.05
	507.5	11.6 ± 0.4	4.5 ± 0.4	7.1 ± 0.5	135.4 ± 11.1	92.5 ± 3.56	0.33 ± 0.04
TBC1	5	83.5 ± 2.0	2.8 ± 0.3	81.1 ± 2.0	2 ± 2.0	2.4 ± 0.6	0.21 ± 0.05
	55	84.7 ± 4.4	2.9 ± 0.4	76.8 ± 4.1	7 ± 1.3	9.9 ± 0.9	0.18 ± 0.02
	105	33.1 ± 1.2	10.8 ± 0.8	20.9 ± 1.3	20 ± 2.4	23.6 ± 0.9	0.20 ± 0.01
	155	28.2 ± 1.0	6.9 ± 0.6	21.4 ± 1.2	31 ± 4.5	32.8 ± 0.9	0.23 ± 0.01
	205	24.5 ± 0.8	8.0 ± 0.7	15.4 ± 1.0	43 ± 4.9	43.5 ± 1.0	0.24 ± 0.01
	255	15.4 ± 0.5	4.4 ± 0.3	11.0 ± 0.6	59 ± 7.0	59.5 ± 1.0	0.24 ± 0.00
	305	13.2 ± 0.4	5.4 ± 0.4	7.7 ± 0.6	75 ± 8.7	78.9 ± 1.1	0.23 ± 0.00
	355	8.7 ± 0.4	5.5 ± 0.4	3.2 ± 0.6	98 ± 11.3	114.1 ± 1.3	0.21 ± 0.00

(TBC1 and TBC5) are 4.1 and 3.8 mm/yr, increasing to 4.7 and 4.0 mm/yr since 1990.

3.4. Hydro-period

LiDAR data indicated the lowest elevation of the berm at the seaward edge of the mangrove basin is 0.55 m AHD (Fig. 2A). The pressure loggers placed around the basin show flooding of the site occurred at high tides equivalent to ≥0.68 m AHD, as recoded at the Terranora tide gauge station (AWRC No. 201447). This difference implies there is approximately 0.1 m of tidal attenuation between the gauge site and studied mangrove basin. The mangrove basin flood tide height therefore represents the 90th percentile of all high tides (Fig. 4A). This equates to an average of approximately 61 high tides/year with tidal inundation tracking the lunar spring-tide cycle.

4. Discussion

In the following discussion the mode of substrate accumulation is first examined, then the rates of substrate accretion are compared with regional and local SLR. Lastly, the implications of substrate accretion for C sequestration are discussed.

4.1. Modes of mangrove substrate production

Mangrove substrate growth has been attributed to both sediment accretion (Lovelock et al., 2015) and biological production (McKee et al., 2007; Toscano and Macintyre, 2003). Sediment accretion is a major component of mangrove substrate vertical accretion in some environments (Cahoon and Lynch, 1997), including in Moreton Bay, ~80 km north of the study site (Lovelock et al., 2015). It has been suggested that if sediment accretion is lower than SLR mangroves may collapse (Ellison and Stoddart, 1991). In other settings, however, such as the Caribbean, peat/root production appears to be the main means of substrate growth (McKee et al., 2007; Parkinson et al., 1994).

At the study site, the contribution of sediment accretion versus biological production was determined from the difference between sediment depth and the sedimentation rate. In TBC6 the difference between the ^{210}Pb CRS model mass accumulation rate (the sedimentation rate) and the sediment depth demonstrated that substrate in the upper 300 mm of core consists primarily of an organic matrix. The physical component of the core (including sediment and organic matter) equates to only 34 mm (11%) of the vertical core space. Within this 34 mm, approximately 60% consisted of organic matter with the remainder mineral sediment. The main component of the vertical height of the core therefore consists of void (89%), indicating the structure of the substrate

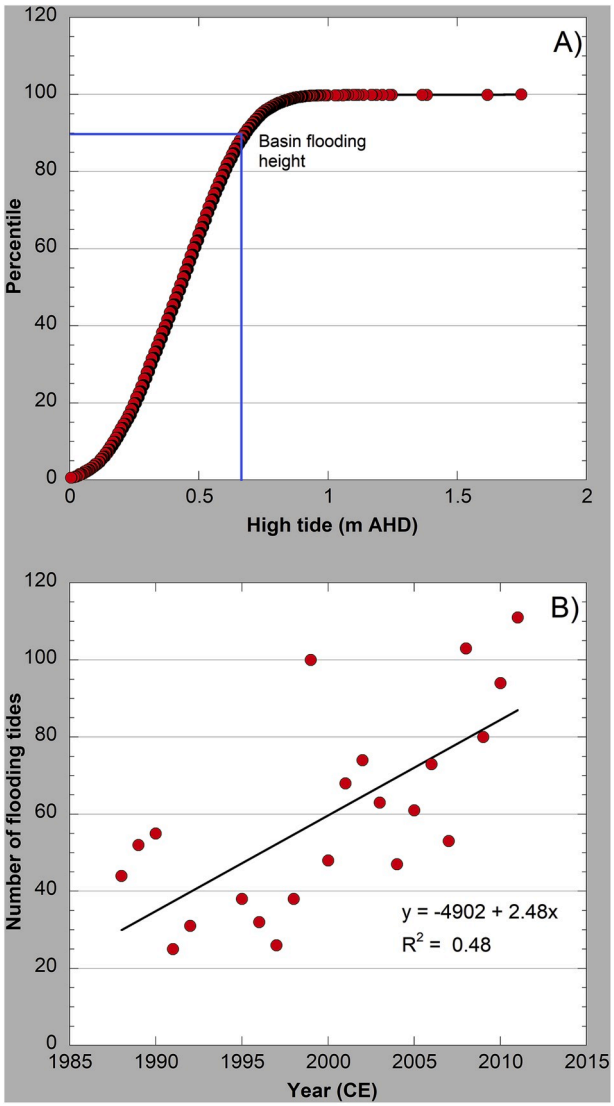

Fig. 4. Hydro-period at the study site. A) High tide percentiles for the Terranorra tide gauge station (AWRC No. 201447). The level at which the tides connect to the studied mangrove basin is indicated by the blue line. B) The number of high tides per annum which connect to the mangrove basin. (For interpretation of the references to colour in this figure legend, the reader is referred to the Web version of this article.)

is being supported by an organic matrix as evident in the core image (Fig. 3A) and indicated by the very low bulk densities in the upper 300 mm of the core (Fig. 3C). This is consistent with the upper part of the substrate being developed from mangrove roots, which are known to respond to tidal inundation (Baylis, 1950; Parkinson et al., 1994).

Mangrove peat production has been the dominate mode of substrate production at the study site over the past 70 years. Before 1940 CE sediment accretion was the main mode of substrate production (Fig. 3). The silt unit deposited before 1940 CE largely consists of physical material. It is 65% physical mass (mineral matter and organic matter) of which 74% is mineral material. The change in the mode of substrate development to peat formation beginning after 1940 CE indicates the development of the mangrove basin and coincides with human modification of the Tweed estuary. Dredging and river training occurred downstream of the study site from the early 20th Century. Drainage ditches (for pasture conversion) were constructed adjacent to the study site after the 1960s. These changes would have resulted in increasing hydro-period at the site, facilitating development of the mangrove basin and causing rapid expansion in mangroves in Terranora Broadwater. Mangrove extent almost doubled between the 1930s (48.61 ha) and the late 1940s (91.78 ha), which was much greater than in subsequent periods (Saintilan, 1998).

4.2. Comparison of mangrove substrate accretion to sea level rise

The Fort Denison SL record is the closest SL record to the study site. It records average annual SLR between 1914 and 2013 of 1 mm/yr. This is lower than the centennial-scale substrate accretion rates exhibited in the studied mangrove basin of 4.1–4.5 mm/yr. Rates in the basin are also more than double centennial observations from global composite records of 1.9 mm/yr (1880–2013) (Church and White, 2011). However, SLR in specific locations can vary significantly from global averages (see below), while it is noteworthy that substrate accretion rates calculated from sediment cores in other studies, including in Brazil and southern Florida, also exceed rates of global/regional SRL (Sanders et al., 2010; Smoak et al., 2013).

Because SLR in specific locations can vary significantly from global averages (see below), regional and local SL records may provide a more relevant comparison from which to assess changes at the study site. As noted, the most accurate SL observations in Australia are recorded at ABSLMP sites since the 1990s. The Rosslyn Bay and Port Kembla ABSLMP sites (the closest to Terranora Broadwater) record SLR of 3.5 and 2.6 mm/yr since ~1991 CE (National Tide Centre, 2012). This is significantly lower than the 7.8 to 7.2 mm/yr in the studied mangrove basin over the same period. This difference implies i) substrate production at the study site is occurring faster than SLR, and/or, ii) local SLR differs from global or regional comparisons, and/or, iii) subsidence is affecting the elevation of the study site relative to SL, i.e., substrate growth maybe tuned to regional SLR.

ABSLMP SLR observations from Australia range from 2.6 to 9 mm/yr (National Tide Centre, 2012), indicating there is significant regional variability in SLR. Therefore local tide gauge data may better account for changes at the study site. SL data from the Gold Coast Seaway (28 km north), are not corrected for other factors that may influence SL, however, many of these factors, like climate variability, would also be expected to affect water levels at the study site. The Gold Coast Seaway gauge records SLR of 4.5 mm/yr between 1999 and 2012, similar to the centennial growth rates recoded at the study site. SLR at the Gold Coast increased to 6.9 mm/yr between 2002 and 2012, again comparable to substrate growth in TBC6. This suggests substrate production in the studied mangrove basin matches local SLR. The Brisbane Bar tide gauge records a similar magnitude of SLR to the Gold Coast Seaway (data not shown), implying rates of local SLR are faster than regional estimates. This result illustrates the potential difficulty of using regional SL records to compare with the response at specific sites.

4.3. The effect of subsurface processes on apparent substrate accretion

The surface elevation of mangrove substrate can be influenced by a number of processes operating over different time scales. Longer-term processes include deep subsidence/sedimentary compaction and glacio/hydro isostatic adjustment (Krauss et al., 2014; Murray-Wallace and Woodroffe, 2014), while shorter-term processes include changes in groundwater/water-table and sediment supply, in addition to near-surface sediment compaction, oxidation and biogeochemical decay (Lovelock et al., 2011; Murray-Wallace and Woodroffe, 2014; Rogers et al., 2014; Xiong et al., 2019). Consequently, the substrate can exhibit apparent growth while compacting at greater depth. Alternatively, substrate may exhibit an increase in elevation without a change in mass, e.g., due to a rising water table.

The upper part of the substrate, that is, Units 1 and 2 in core TBC6, represents the most active part of the substrate, containing a high volume of pore space and living and dead organic matter (Fig. 3A and C). It is therefore the region most likely to experience compaction/expansion processes. Calculated vertical growth rates in TBC6 are therefore the net

result of changes in sediment supply, biological production, oxidation and biogeochemical decay. Compaction processes are unlikely to have any significant effect on the active layer of the substrate at the study site. Compaction would manifest as an increase in bulk density or in mass accumulation rates (MAR) in substrate (where MAR = the depth interval divided by time, multiplied by the bulk density). Neither parameter displays any down core pattern in the mangrove peat unit, i.e., bulk density ranges between 0.09 and 0.15 g/m^3, (Std = 0.018) and MARs are between 0.63 and 0.95 g/cm^2/yr (Std = 0.13). Although bulk density and MARs increase within the organic silt unit below the peat this is consistent with a different set of depositional processes, rather than any change in compaction.

Deep subsidence at the study site is expected to be low. Subsidence/compaction rates in eastern Australia are less than −0.01 mm/yr over the Quaternary (Roy and Thom, 1981), much lower than substrate growth rates. The base of the active sedimentary layer consists of a well sorted saturated sand (at 830 mm depth for core TBC6), likely to have relatively low compressibility when combined with the small overburden (<1 m of sediment). The results from SET studies from eastern Australia provide additional information on potential rates of subsidence/compaction that could occur below the depth of the collected cores. However, much of the compaction recorded in SET studies would be expected to occur in the upper part of the substrate profile and is therefore already included in our calculated substrate accretion rates for the study site. In addition, SETs have other limitations. For example, it is assumed the central control rod remains stable, while SET elevation changes are also influenced by antecedent water (rainfall and water levels) (Rogers et al., 2014). Despite these limitations, the relatively wide spatial extent of SET studies in eastern Australia provides a useful approximation of broad-scale compaction. Across eastern Australia, expansion (+)/compaction (−) measured by SETs ranges from +0.19 (measured in the Tweed estuary downstream of the study site) to −11.6 (measured on the Victorian south-coast (Rogers et al., 2006). If the average eastern Australian sediment compaction rate of −2.5 mm/yr (n = 23) were occurring at the study site, the resultant vertical substrate accretion would occur at a similar rate to regional SLR, but below local SLR rates. Applying the locally measured rate of substrate expansion measured in the Tweed estuary (+0.19 mm/yr) results in little difference to the calculated core growth rates, i.e., the surface elevation change would remain similar to local SLR estimates. Overall, it is unlikely subsidence/compaction are influencing the study site below the depth of the cores. Consequently, the studied substrate is accreting coincident to SLR.

4.4. *Living landscapes? Feedbacks between mangrove substrate and hydro-period*

Agreement between the master-core growth rate and SLR since the late 1990s implies enhanced subsurface production occurs in response to increased hydro-period (conceptualised in Fig. 5), with mangrove production known to respond to inundation (Baylis, 1950; McKee et al., 2007; Parkinson et al., 1994; Rogers et al., 2019). The Terranora tide gauge (AWRC No. 201447) demonstrates that high tides exceeding the mangrove basin flood height (0.68 m) have been increasing by ~2/year between 1987 and 2011 (Fig. 4B), likely driving increased mangrove substrate production. This negative feedback allows mangrove basins to persist in the highly dynamic coastal environment, where changes in hydro-period are caused by a variety of processes in addition to SL change, e.g., coastal geomorphic and fluvial reorganisation, increased sedimentation, or neotectonics. This is shown, for example, in the Caribbean and Gulf of Mexico (intermediate field sites) where peat sequences of up to 18 m deep have tracked Holocene SLR (Toscano and Macintyre, 2003) and by rapid production of organic substrate in eastern Australia following mining subsidence (Rogers et al., 2019).

While the initial change to organic dominated root production at the study site may have been caused by human modification of hydro-period, substrate production since that time is likely the result of ongoing SLR (Fig. 5). Development of substrate across the mangrove basin suggests the basin is maintaining the same position within the tidal plane, where the site remains flooded by high tides above the 90th percentile, tracking an increase in SL (e.g., Fig. 5c).

We hypothesise the trigger for subsurface production is reduced dissolved oxygen (DO) during tidal inundation. DO in pool water at the study site decreases to 0 mg/l within a few hours following a tidal

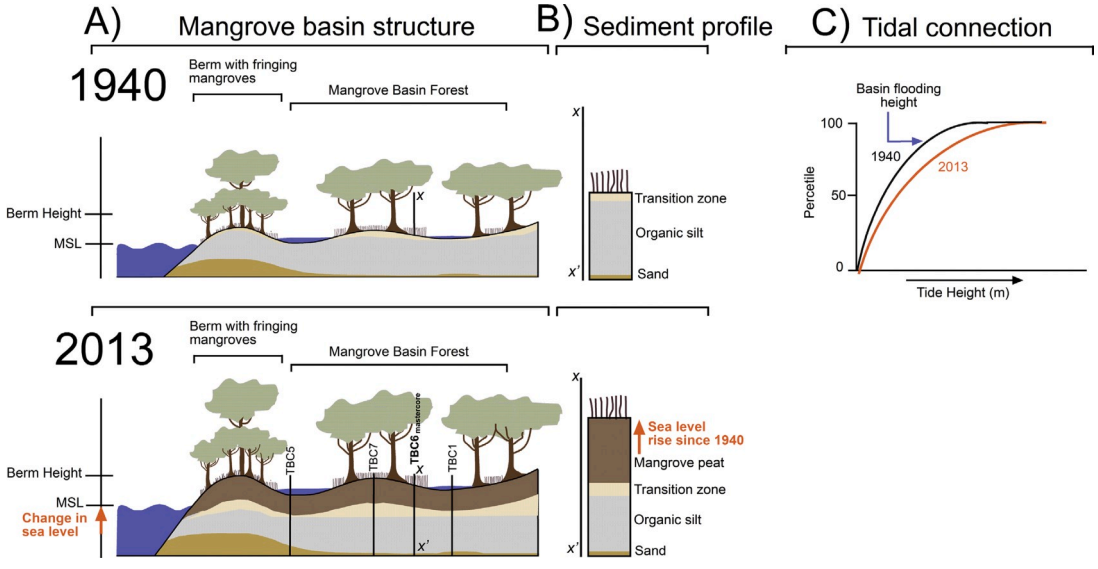

Fig. 5. Conceptual diagram showing the response of the studied mangrove basin forest to changing sea level. A) Top panel shows the substrate height and structure as it would have been in at 1940 CE, before significant human modification (as inferred from core stratigraphy). The lower panel shows the degree of sedimentary development by 2013 CE. After 1940 CE the mode of substrate production changed becoming dominated by organic production and resulting in 400 mm of mangrove peat formation. The figure shows the rate of mangrove peat production occurs at a rate broadly matching sea level rise, as indicated by the red arrow on the left of the lower panel. Panel B shows the change in structure and degree of substrate accretion between 1940 and 2013. Panel C shows the theoretical change to hydro-period between 1940 and 2013. Note, that although sea level increases, vertical accretion of mangrove substrate results in the mangrove basin maintaining the same position within the tidal plane. (For interpretation of the references to colour in this figure legend, the reader is referred to the Web version of this article.)

connection (Knight et al., 2013), while low DO levels have been recorded within pneumatophores during inundation (Allaway et al., 2001). Therefore low DO levels during pneumatophore inundation may trigger mangrove root growth (Baylis, 1950; McKee et al., 2007; Parkinson et al., 1994; Rogers et al., 2019). Further research is needed to test this relationship.

4.5. Carbon sequestration

Mangroves incorporate large amounts of CO_2, into their biomass or substrate (Rogers et al., 2019). Because they build organic substrate their ability to sequester C below ground is of particular significance (Alongi, 2014). The growth of peat sequences in response to increased hydro-period therefore represents a negative feedback to human induced SLR via drawdown and sequestration of atmospheric CO_2.

In the study site, the rate of C sequestration can be estimated from the organic matter content of the evolving peat sequence. In broad terms, C comprises approximately 50% of organic matter (Howard and Howard, 1990; Pribyl, 2010). Consequently, the studied mangrove basin forest has sequestered C at a rate of >220 g/m^2/yr over the past 100 years (as calculated from TBC6), comparable, although higher, than the average global rate of mangrove C sequestration of 174 g/m^2/yr (Alongi, 2014). Rates of C sequestration calculated in this study are also comparable with, although towards the upper end of, C sequestration measured in 24 mangrove systems across Australia at an average of 126 ± 90 g/m^2/yr (Serrano et al., 2019). We suspect the relatively high rates of C sequestration measured in this study are due to the study site being a mangrove basin, which may have the ability to sequester more C by comparison to mangroves in other geomorphic configurations. Organic content in TBC6 increased after ~1970 CE suggesting C storage represents a negative feedback to atmospheric $C0_2$ levels from SLR within some mangrove systems.

Accurately assessing the rate of C sequestration in mangroves is complex as some of the peat may be living, i.e., part of the substrate is comprised of active roots. This is unlike other peats, which often have very shallow rooted vegetation, e.g. alpine peatlands or sphagnum peat. This obviously affects the ability to constrain rates of C sequestration. Despite this limitation, in the upper peat unit across the Terranora site, rates of C sequestration approximates 250–300 g/m^2/yr since the late 1990s, confirming the results of recent studies which demonstrate increasing C sequestration in response to increasing hydro-period (Rogers et al., 2019).

5. Summary and implications

This study demonstrates root production is the main means of surface accretion at the study site, resulting in surface growth rates of approximately 4 mm/yr over the past century. The rate of vertical substrate production is broadly consistent with local and regional measures of SLR, while increasing subsurface accretion after ~1990 CE is also consistent with local increases in SLR from this time.

Our results indicate mangrove basin forests may, in some cases, be resilient to SLR. This is because mangroves occupy a dynamic coastal environment where hydro-period can be influenced by processes independent of SLR and human activity, e.g., rainfall variability, coastal geomorphic change. To exist in this dynamic space, mangrove basin forests have adapted ecogeomorphic feedbacks that allow them to respond rapidly to changing conditions, that is, building organic substrate during increased tidal inundation or oxidation/collapse of organic substrate if tidal inundation decreases. Although it should also be noted palaeo records show there are limits to mangrove resilience (Woodroffe et al., 2016).

Substrate production at the study site is also resulting in significant C sequestration. This further confirms the capacity of mangrove systems to act as a negative feedback to global warming via atmospheric CO_2 drawdown and C storage.

Declaration of competing interest

The authors declare that they have no known competing financial interests or personal relationships that could have appeared to influence the work reported in this paper.

CRediT authorship contribution statement

Samuel K. Marx: Conceptualization, Methodology, Formal analysis, Resources, Writing - original draft, Writing - review & editing, Project administration, Funding acquisition. **Jon M. Knight:** Conceptualization, Methodology, Formal analysis, Resources, Writing - review & editing, Project administration, Funding acquisition. **Patrick G. Dwyer:** Conceptualization, Methodology, Formal analysis, Resources, Writing - review & editing, Funding acquisition. **David P. Child:** Methodology, Resources, Writing - review & editing, Formal analysis, Funding acquisition. **Michael A.C. Hotchkis:** Methodology, Resources, Formal analysis, Funding acquisition. **Atun Zawadzki:** Methodology, Resources, Formal analysis, Funding acquisition.

Acknowledgments

Financial support from the Australian Government for the Centre for Accelerator Science at ANSTO through the National Collaborative Research Infrastructure Strategy (NCRIS) is acknowledged. Australian Institute of Nuclear Science and Engineering Awards ALNGRA10115, ALNGRA13052, ALNGRA14534 supported the geochronological analysis. We thank Jack Goralewski for processing the ^{210}Pb samples. We acknowledge the ongoing support of Tweed Shire Council, both financially and in-kind, and particularly Brian Falkner for his insights and ongoing advice and for negotiating access to the study site since 2009. Finally we thank two anonymous reviewers whose comments improved this manuscript.

Appendix A. Supplementary data

Supplementary data to this article can be found online at https://doi.org/10.1016/j.ecss.2020.106813.

References

Allaway, W.G., Curran, M., Hollington, L.M., Ricketts, M.C., Skelton, N.J., 2001. Gas space and oxygen exchange in roots of *Avicennia marina* (Forssk.) Vierh. var. australasica (Walp.) Moldenke ex N. C. Duke, the Grey Mangrove. Wetl. Ecol. Manag. 9, 221–228.

Alongi, D.M., 2014. Carbon cycling and storage in mangrove forests. Annu. Rev. Marine Sci. 6, 195–219.

Appleby, P.G., Oldfield, F., 1978. The calculation of lead-210 dates assuming a constant rate of supply of unsupported 210Pb to the sediment. Catena 5, 1–8.

Baylis, G.T.S., 1950. Root system of the New Zealand mangrove. Trans. R. Soc. N. Z. 78, 509–514.

Beaman, R., Larcombe, P., Carter, R.M., 1994. New evidence for the Holocene sea-level high from the inner shelf, central Great Barrier Reef, Australia. J. Sediment. Res. 64, 881–885.

Boumans, R.M.J., Day, J.W., 1993. High precision measurements of sediment elevation in shallow coastal areas using a sedimentation-erosion table. Estuaries 16, 375–380.

Breithaupt, J.L., Smoak, J.M., Byrne, R.H., Waters, M.N., Moyer, R.P., Sanders, C.J., 2018. Avoiding timescale bias in assessments of coastal wetland vertical change. Limnol. Oceanogr. 63, S477–S495.

Cahoon, D.R., Hensel, P., Rybczyk, J., McKee, K.L., Proffitt, C.E., Perez, B.C., 2003. Mass tree mortality leads to mangrove peat collapse at Bay Islands, Honduras after Hurricane Mitch. J. Ecol. 91, 1093–1105.

Cahoon, D.R., Lynch, J.C., 1997. Vertical accretion and shallow subsidence in a mangrove forest of southwestern Florida. U.S.A. Mangroves and Salt Marshes 1, 173–186.

Cahoon, D.R., Lynch, J.C., Hensel, P., Boumans, R., Perez, B.C., Segura, B., Day Jr., J.W., 2002. High-precision measurements of wetland sediment elevation. I. Recent improvements to the sedimentation-erosion table. J. Sediment. Res. 72, 730–733.

Cahoon, D.R., Turner, R.E., 1989. Accretion and canal impacts in a rapidly subsiding wetland: II. Feldspar marker horizon technique. Estuaries 12, 260–268.

Child, D.P., Hotchkis, M.A.C., Williams, M.L., 2008. High sensitivity analysis of Plutonium isotopes in environmental samples using Accelerator Mass Spectrometry (AMS). J. Anal. Atomic Spectrom. 23, 765–768.

Church, J., White, N., 2011. Sea-level rise from the late 19th to the early 21st century. Surv. Geophys. 32, 585–602.
Duke, N., 2006. Australia's Mangroves, the Authoritative Guide to Australia's Mangrove Plants. The University of Queensaland.
Duke, N.C., Meynecke, J.O., Dittmann, S., Ellison, A.M., Anger, K., Berger, U., Cannicci, S., Diele, K., Ewel, K.C., Field, C.D., Koedam, N., Lee, S.Y., Marchand, C., Nordhaus, I., Dahdouh-Guebas, F., 2007. A world without mangroves? Science 41.
Ellison, J.C., 1993. Mangrove retreat with rising sea-level. Bermuda. Estuar. Coast Shelf Sci. 37, 75–87.
Ellison, J.C., Stoddart, D.R., 1991. Mangrove ecosystem collapse during predicted sea-level rise: Holocene analogues and implications. J. Coast Res. 7, 151–165.
Faunce, C.H., Serafy, J.E., 2006. Mangroves as fish habitat: 50 years of field studies. Mar. Ecol. Prog. Ser. 318, 1–18.
Field, C.D., 1995. Impact of expected climate change on mangroves. Hydrobiologia 295, 75–81.
Field, E., Marx, S., Haig, J., May, J.H., Jacobsen, G., Zawadzki, A., Child, D., Heijnis, H., Hotchkis, M., McGowan, H., Moss, P., 2018. Untangling geochronological complexity in organic spring deposits using multiple dating methods. Quat. Geochronol. 43, 50–71.
Hancock, G.J., Leslie, C., Everett, S.E., Tims, S.G., Brunskill, G.J., Haese, R., 2011. Plutonium as a chronomarker in Australian and New Zealand sediments: a comparison with ^{137}Cs. J. Environ. Radioact. 102, 919–929.
Horton, B.P., Gibbard, P.L., Mine, G.M., Morley, R.J., Purintavaragul, C., Stargardt, J.M., 2005. Holocene sea levels and palaeoenvironments, Malay-Thai Peninsula, southeast Asia. Holocene 15, 1199–1213.
Howard, P.J.A., Howard, D.M., 1990. Use of organic carbon and loss-on-ignition to estimate soil organic matter in different soil types and horizons. Biol. Fertil. Soils 9, 306–310.
Kaplan, D.I., Powell, B.A., Gumapas, L., Coates, J.T., Fjeld, R.A., Diprete, D.P., 2006. Influence of pH on plutonium desorption/solubilization from sediment. Environ. Sci. Technol. 40, 5937–5942.
Ketterer, M.E., Groves, A.D., Strick, B.J., Asplund, C.S., Jones, V.J., 2013. Deposition of ^{236}U from atmospheric nuclear testing in Washington state (USA) and the Pechora region (Russian Arctic). J. Environ. Radioact. 118, 143–149.
Knight, J., Griffin, L., Dale, P., Phinn, S., 2012. Oviposition and larval habitat preferences of the saltwater mosquito, *Aedes vigilax*, in a subtropical mangrove forest in Queensland, Australia. J. Insect Sci. 12, 6-6.
Knight, J.M., 2011. A model of mosquito–mangrove basin ecosystems with implications for management. Ecosystems 14, 1382–1395.
Knight, J.M., Dale, P.E.R., Dunn, R.J.K., Broadbent, G.J., Lemckert, C.J., 2008. Patterns of tidal flooding within a mangrove forest: Coombabah Lake, southeast Queensland, Australia. Estuar. Coast Shelf Sci. 76, 580–593.
Knight, J.M., Dale, P.E.R., Spencer, J., Griffin, L., 2009. Exploring LiDAR data for mapping the micro-topography and tidal hydro-dynamics of mangrove systems: an example from southeast Queensland, Australia. Estuar. Coast Shelf Sci. 85, 593–600.
Knight, J.M., Griffin, L., Dale, P.E.R., Sheaves, M., 2013. Short-term dissolved oxygen patterns in sub-tropical mangroves. Estuar. Coast Shelf Sci. 131, 290–296.
Koch, E.W., Barbier, E.B., Silliman, B.R., Reed, D.J., Perillo, G.M.E., Hacker, S.D., Granek, E.F., Primavera, J.H., Muthiga, N., Polasky, S., Halpern, B.S., Kennedy, C.J., Kappel, C.V., Wolanski, E., 2009. Non-linearity in ecosystem services: temporal and spatial variability in coastal protection. Front. Ecol. Environ. 7, 29–37.
Krauss, K.W., McKee, K.L., Lovelock, C.E., Cahoon, D.R., Saintilan, N., Reef, R., Chen, L., 2014. How mangrove forests adjust to rising sea level. New Phytol. 202, 19–34.
Laurance, W.F., Dell, B., Turton, S.M., Lawes, M.J., Hutley, L.B., McCallum, H., Dale, P., Bird, M., Hardy, G., Prideaux, G., Gawne, B., McMahon, C.R., Yu, R., Hero, J.M., Schwarzkopf, L., Krockenberger, A., Douglas, M., Silvester, E., Mahony, M., Vella, K., Saikia, U., Wahren, C.H., Xu, Z., Smith, B., Cocklin, C., 2011. The 10 Australian ecosystems most vulnerable to tipping points. Biol. Conserv. 144, 1472–1480.
Lewis, S.E., Sloss, C.R., Murray-Wallace, C.V., Woodroffe, C.D., Smithers, S.G., 2013. Post-glacial sea-level changes around the Australian margin: a review. Quat. Sci. Rev. 74, 115–138.
Longmore, M., O'Leary, B., Rose, C., Chandica, A., 1983. Mapping soil erosion and accumulation with the fallout isotope caesium-137. Soil Res. 21, 373–385.
Lovelock, C., Bennion, V., Grinham, A., Cahoon, D., 2011. The role of surface and subsurface processes in keeping pace with sea level rise in intertidal wetlands of Moreton Bay, Queensland, Australia. Ecosystems 14, 745–757.
Lovelock, C.E., Cahoon, D.R., Friess, D.A., Guntenspergen, G.R., Krauss, K.W., Reef, R., Rogers, K., Saunders, M.L., Sidik, F., Swales, A., Saintilan, N., Thuyen, L.X., Triet, T., 2015. The vulnerability of Indo-Pacific mangrove forests to sea-level rise. Nature 526, 559–563.
Lugo, A.E., Snedaker, S.C., 1974. The ecology of mangroves. Annu. Rev. Ecol. Systemat. 5, 139–160.
Lynch, J.C., Meriwether, J.R., McKee, B.A., Vera-Herrera, F., Twilley, R.R., 1989. Recent accretion in mangrove ecosystems based on ^{137}Cs and ^{210}Pb. Estuaries 12, 284–299.
McKee, K.L., Cahoon, D.R., Feller, I.C., 2007. Caribbean mangroves adjust to rising sea level through biotic controls on change in soil elevation. Global Ecol. Biogeogr. 16.
Murray-Wallace, C.V., Woodroffe, C.D., 2014. Quaternary Sea-Level Changes, A Global Perspective. Cambridge University Press.
Murray, A.B., Knaapen, M.A.F., Tal, M., Kirwan, M.L., 2008. Biomorphodynamics: physical-biological feedbacks that shape landscapes. Water Resour. Res. 44 (11).
National Tide Centre, 2012. Monthly Data Report December 2012; Australian Baseline Sea Level Monitoring Array, pp. 1–30.
Parkinson, W.R., DeLaune, R.D., White, J.R., 1994. Holocene sea-level rise and the fate of mangrove forests within the wider Caribbean region. J. Coast Res. 10, 1077–1086.
Pérez, A., Machado, W., Gutierrez, D., Stokes, D., Sanders, L., Smoak, J.M., Santos, I., Sanders, C.J., 2017. Changes in organic carbon accumulation driven by mangrove expansion and deforestation in a New Zealand estuary. Estuar. Coast Shelf Sci. 192, 108–116.
Pribyl, D.W., 2010. A critical review of the conventional SOC to SOM conversion factor. Geoderma 156, 75–83.
Purnobasuki, H., 2013. Characteristics of root caps in four root types of *Avicennia marina* (forsk.) vierh. Am. J. Plant Sci. 4, 853–858.
Robbins, J.A., Edgington, D.N., 1975. Determination of recent sedimentation rates in Lake Michigan using Pb-210 and Cs-137. Geochem. Cosmochim. Acta 39, 285–304.
Rogers, K., Kelleway, J.J., Saintilan, N., Megonigal, J.P., Adams, J.B., Holmquist, J.R., Lu, M., Schile-Beers, L., Zawadzki, A., Mazumder, D., Woodroffe, C.D., 2019. Wetland carbon storage controlled by millennial-scale variation in relative sea-level rise. Nature 567, 91–95.
Rogers, K., Saintilan, N., Woodroffe, C.D., 2014. Surface elevation change and vegetation distribution dynamics in a subtropical coastal wetland: implications for coastal wetland response to climate change. Estuar. Coast Shelf Sci. 149, 46–56.
Rogers, K., Wilton, K.M., Saintilan, N., 2006. Vegetation change and surface elevation dynamics in estuarine wetlands of southeast Australia. Estuar. Coast Shelf Sci. 66, 559–569.
Roy, P.S., Thom, B.G., 1981. Late quaternary marine deposition in New South Wales and southern Queensland: an evolutionary model. J. Geol. Soc. Aust. 28, 471–489.
Saintilan, N., 1998. Photogrammetric survey of the Tweed River wetlands. Wetlands 17, 74–82.
Sanders, C.J., Smoak, J.M., Sanders, L.M., Waters, M.N., Patchineelam, S.R., Ketterer, M. E., 2010. Intertidal mangrove mudflat $^{240+239}$Pu signatures, confirming a ^{210}Pb geochronology on the southeastern coast of Brazil. J. Radioanal. Nucl. Chem. 283, 593–596.
Sasmito, S.D., Murdiyarso, D., Friess, D.A., Kurnianto, S., 2016. Can mangroves keep pace with contemporary sea level rise?: A global data review. Wetl. Ecol. Manag. 24, 263–278.
Scholl, D.W., Stuiver, M., 1967. Recent submergence of southern Florida: a comparison with adjacent coasts and other eustatic data. Ecol. Soc. Am. Bull. 78, 437–454.
Scholl, O.W., Craighead, F.C., Stuiver, I., 1969. Florida submergence curve revised: its relation to coastal sedimentation rates. Science 163, 562–564.
Serrano, O., Lovelock, C.E., Atwood, T., Macreadie, P.I., Canto, R., Phinn, S., Arias-Ortiz, A., Bai, L., Baldock, J., Bedulli, C., Carnell, P., Connolly, R.M., Donaldson, P., Esteban, A., Ewers Lewis, C.J., Eyre, B.D., Hayes, M.A., Horwitz, P., Hutley, L.B., Kavazos, C.R.J., Kelleway, J.J., Kendrick, G.A., Kilminster, K., Lafratta, A., Lee, S., Lavery, P.S., Maher, D.T., Marbà, N., Masque, P., Mateo, M.A., Mount, R., Ralph, P. J., Roelfsema, C., Rozaimi, M., Ruhon, R., Salinas, C., Samper-Villarreal, J., Sanderman, J., Sanders, C., Santos, I., Sharples, C., Steven, A.D.L., Cannard, T., Trevathan-Tackett, S.M., Duarte, C.M., 2019. Australian vegetated coastal ecosystems as global hotspots for climate change mitigation. Nat. Commun. 10, 4313.
Sloss, C.R., Murray-Wallace, C.V., Jones, B.G., 2007. Holocene sea-level change on the southeast coast of Australia: a review. Holocene 17, 999–1014.
Smoak, J.M., Breithaupt, J.L., Smith, T.J., Sanders, C.J., 2013. Sediment accretion and organic carbon burial relative to sea-level rise and storm events in two mangrove forests in Everglades National Park. Catena 104, 58–66.
Srncik, M., Tims, S.G., De Cesare, M., Fifield, L.K., 2014. First measurements of ^{236}U concentrations and ^{236}U/^{239}Pu isotopic ratios in a Southern Hemisphere soil far from nuclear test or reactor sites. J. Environ. Radioact. 132, 108–114.
Thom, B.G., Roy, P.S., 1985. Relative sea-levels and coastal sedimentation in southeast Australia in the Holocene. J. Sediment. Petrol. 55, 257–264.
Toscano, M.A., Macintyre, I.G., 2003. Corrected western Atlantic sea-level curve for the last 11,000 years based on calibrated C-14 dates from *Acropora palmata* framework and intertidal mangrove peat. Coral Reefs 22, 257–270.
Twilley, R.R., Rivera-Monroy, V.H., Rovai, A.S., Castañeda-Moya, E., Davis, S., 2019. Chapter 21 - mangrove biogeochemistry at local to global scales using ecogeomorphic approaches. In: Perillo, G.M.E., Wolanski, E., Cahoon, D.R., Hopkinson, C.S. (Eds.), Coastal Wetlands. Elsevier, pp. 717–785.
UNSCEAR, 2000. Sources and Effects of Ionizing Radiation. United Nations, Vienna, Austria, p. 649.
Urban, N.R., Eisenreich, S.J., Grigal, D.F., Schurr, K.T., 1990. Mobility and diagenesis of Pb and ^{210}Pb in peat. Geochem. Cosmochim. Acta 54, 3329–3346.
Vo, Q.T., Kuenzer, C., Vo, Q.M., Moder, F., Oppelt, N., 2012. Review of valuation methods for mangrove ecosystem services. Ecol. Indicat. 23, 431–446.
Wendel, C.C., Oughton, D.H., Lind, O.C., Skipperud, L., Fifield, L.K., Isaksson, E., Tims, S. G., Salbu, B., 2013. Chronology of Pu isotopes and ^{236}U in an Arctic ice core. Sci. Total Environ. 461–462, 734–741.
Wilcken, K.M., Hotchkis, M., Levchenko, V., Fink, D., Hauser, T., Kitchen, R., 2015. From carbon to actinides: a new universal 1MV accelerator mass spectrometer at ANSTO. Nucl. Instrum. Methods Phys. Res. Sect. B Beam Interact. Mater. Atoms 361, 133–138.
Wolanski, E., 2007. Estuarine Ecohydrology. Elsevier, Amsterdam, The Netherlands.
Woodroffe, C.D., 1981. Mangrove swamp stratigraphy and Holocene transgression. Mar. Geol. 41, 271–294.
Woodroffe, C.D., 1990. The impact of sea-level rise on mangrove shorelines. Prog. Phys. Geogr. 14, 483–520.
Woodroffe, C.D., 2007. Critical thresholds and the vulnerability of Australian tropical coastal ecosystems to the impacts of climate change. J. Coast Res. 464–468.
Woodroffe, C.D., Lovelock, C.E., Rogers, K., 2015. Mangrove Shorelines, Coastal Environments and Global Change, pp. 251–267.
Woodroffe, C.D., Mulrennan, M.E., Chappell, J., 1993. Estuarine infill and coastal progradation, southern Van-Diemen Gulf, northern Australia. Sediment. Geol. 83, 257–275.

Woodroffe, C.D., Rogers, K., McKee, K.L., Lovelock, C.E., Mendelssohn, I.A., Saintilan, N., 2016. Mangrove sedimentation and response to relative sea-level rise. Annu. Rev. Marine Sci. 8, 243–266.
Woodroffe, C.D., Thom, B.G., Chappell, J., 1985. Development of widespread mangrove swamps in mid-Holocene times in northern Australia. Nature 317, 711–713.
Xiong, Y., Ola, A., Phan, S.M., Wu, J., Lovelock, C.E., 2019. Soil structure and its relationship to shallow soil subsidence in coastal wetlands. Estuar. Coast 42, 2114–2123.
Zheng, J., Wu, F., Yamada, M., Liao, H., Liu, C., Wan, G., 2008. Global fallout Pu recorded in lacustrine sediments in Lake Hongfeng, SW China. Environ. Pollut. 152, 314–321.